Proc. Int. Conf. Heavy Electrons (ICHE2010)
J. Phys. Soc. Jpn. **80** (2011) SAheavy2010

Continuous-Time Quantum Monte Carlo Study of Local Non-Fermi Liquid State in the Multichannel Anderson Model

Junya Otsuki*

Department of Physics, Tohoku University, Sendai 980-8578

The impurity Green's function G_f in the local non-Fermi liquid state is evaluated by means of the continuous-time quantum Monte Carlo method extended to the multichannel Anderson model. For $N = M$ (where N and M are numbers of spin components and channels, respectively), G_f is expressed as $-\mathrm{Im}G_f(\omega + \mathrm{i}0) = c - b|\omega|^{1/2}$, and the zero-frequency value c depends only on N ($= M$). A corresponding impurity self-energy at low frequencies is composed of two parts: a resonance term related to c, and a non-Fermi liquid term proportional to $|\omega|^{1/2}$. The characteristic energy scale is discussed in terms of the non-Fermi liquid term in the self-energy.

KEYWORDS: continuous-time quantum Monte Carlo (CT-QMC), two-channel Kondo effect

1. Introduction

The multichannel Kondo effect is a typical example that leads to a local non-Fermi liquid ground state.[1)] It has been recognized that the peculiar low-temperature behaviors observed in uranium compounds and metals with uranium impurities are due to the two-channel Kondo effect.[2)] This kind of non-Fermi liquid state has been investigated from a more general point of view based on models generalized to $\mathrm{SU}(N) \otimes \mathrm{SU}(M)$ symmetry.[3)] Then, their critical nature has been discussed extensively.[4,5)]

Regarding the (single-channel) Kondo problem, the Anderson Hamiltonian gives clear insight:[6,7)] the ground state is connected to that in the non-interacting limit. In this analogy, the multichannel Kondo effect can be addressed based on an Anderson Hamiltonian.[8)] The inclusion of the impurity charge degree of freedom enables us to describe the local dynamics via the impurity Green's function. We thus consider the $\mathrm{SU}(N) \otimes \mathrm{SU}(M)$ multichannel Anderson model given by[2)]

$$\mathcal{H} = \sum_{\boldsymbol{k}\alpha\mu} \epsilon_{\boldsymbol{k}} c^\dagger_{\boldsymbol{k}\alpha\mu} c_{\boldsymbol{k}\alpha\mu} + E_{\mathrm{ex}} \sum_{\alpha} X_{\alpha,\alpha} + V \sum_{\alpha\mu} \left(X_{\mu,-\alpha} c_{\alpha\mu} + \mathrm{h.c.} \right). \quad (1)$$

The (pseudo-)spin index μ and channel index α run over N and M components, respectively. The f^2 state $|\mu\rangle$ forms a channel singlet ($-\alpha$ denotes the counterpart of α), and the f^1 state $|\alpha\rangle$ has the energy E_{ex} relative to $|\mu\rangle$. The Hilbert space of f states is restricted to $|\alpha\rangle$ and $|\mu\rangle$ by using the X-operators $X_{\gamma,\gamma'} = |\gamma\rangle\langle\gamma'|$ with $\gamma = \alpha, \mu$, on which $\sum_\gamma X_{\gamma,\gamma} = 1$ is imposed. $c_{\alpha\mu} = N_0^{-1/2} \sum_{\boldsymbol{k}} c_{\boldsymbol{k}\alpha\mu}$ with N_0 being number of sites. The M-channel Coqblin-Schrieffer model is derived from the Hamiltonian (1) as a localized limit $V^2,\ E_{\mathrm{ex}} \to \infty$ with V^2/E_{ex} fixed. Exact thermodynamics of the model (1)[9)] as well as the localized limit[5)] has been derived.

Concerning the dynamical properties, a two-channel case, $N = M = 2$, has been clarified by the numerical renormalization group[10)] and by an exact method.[11)] General cases have been investigated by perturbational treatments.[3,12,13)] In this paper, we numerically investigate the dynamical properties of the multichannel Anderson model. To this end, we develop an algorithm based on the recently developed continuous-time quantum Monte Carlo (CT-QMC) method,[14–16)] which is explained in the next section. We show numerical results for the impurity Green's function and self-energy in §3.

2. CT-QMC for the multichannel Anderson model

We study the model (1) by the CT-QMC, which evaluates a perturbation expansion stochastically. In the present case, we adopt the hybridization expansion.[15)] Since the non-perturbative part is diagonal with respect to α and μ, the efficient algorithm using a 'segment' picture is applicable by a slight modification. Figure 1 shows a diagram of a configuration of order V^6. Spin states μ_i and channel states α_i appear alternately, which are hereafter referred to as segment and anti-segment, respectively. In general, a configuration of order V^{2k} is represented by $q_k \equiv \{\tau_i, \tau'_i, \alpha_i, \mu_i\}$. The trace over the local states is thus taken into account graphically. On the other hand, the trace over conduction electrons is evaluated based on Wick's theorem. A Monte Carlo sampling is performed in the configuration space composed of k and q_k.

We perform the following update processes: (i) addition/removal of a segment or an anti-segment, and (ii) exchange of spin or channel indices. Fig. 2(a) shows the addition of a segment. The index μ of the segment is randomly chosen, and accordingly the update probability differs from that in ref. 15 by a factor of N. When either N or M is larger than 2, the ergodicity is not satisfied only by process (i). For

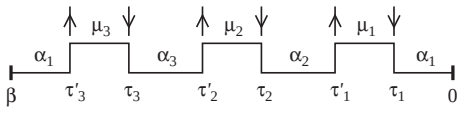

Fig. 1. Diagrammatic representation of a configuration of order V^6. The outgoing and incoming allows indicate creation and annihilation of conduction electrons, respectively.

*E-mail address: otsuki@cmpt.phys.tohoku.ac.jp

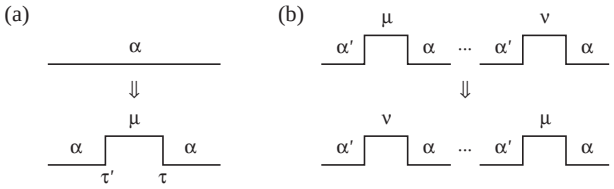

Fig. 2. Update processes: (a) addition of a segment, and (b) exchange of spin indices.

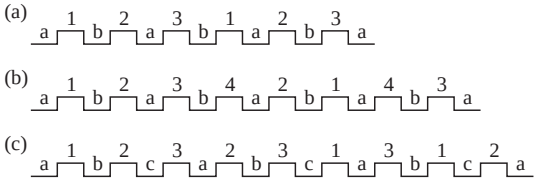

Fig. 3. Examples of diagrams which cannot be reached without the 'exchange' process. The spin and channel components are labeled as 1, 2, $\cdots$, and a, b, $\cdots$, respectively.

example, configurations shown in Fig. 3 cannot be reached. This problem can be solved by introducing a process shown in Fig. 2(b), which exchanges the spin indices. We perform a similar update to exchange the channel indices as well.

In the simulation, we observe negative weight configurations for $N = M > 2$. However, since their contribution is less than 10% in the parameter range shown in this paper, the sign problem has little effect on the simulation.

3. Numerical Results

In this paper, we restrict ourselves to $N = M$. We use a rectangular density of states $\rho(\epsilon) = (1/2D)\theta(D - |\epsilon|)$ for conduction electrons with $D = 1$. We fix $NV^2 = 0.12$ so that the exponent of the Kondo temperature is the same for different N. The width of the localized state $\Delta = \pi V^2 \rho(0)$ is $\Delta \simeq 0.094$ at most (for $N = 2$), and therefore the effect of finite band width may be neglected.

3.1 *Green's function*

We first show results for the single-particle Green's function G_f, which is defined in the restricted Hilbert space by

$$G_f(\mathrm{i}\epsilon_n) = -\int_0^\beta d\tau \langle X_{-\alpha,\mu}(\tau) X_{\mu,-\alpha}\rangle \mathrm{e}^{\mathrm{i}\epsilon_n \tau}, \qquad (2)$$

where $\epsilon_n = (2n+1)\pi T$ is the fermionic Matsubara frequency. At high frequencies, G_f follows $G_f(\mathrm{i}\epsilon_n) \sim a/\mathrm{i}\epsilon_n$ with $a < 1$, since the Hilbert space is restricted. The a varies between $1/N$ and $1/M$ depending on $E_{\rm ex}$, and in a special case of $N = M$, $a = 1/N$.

In Fig. 4, $-\mathrm{Im}G_f(\mathrm{i}\epsilon_n)\Delta$ is plotted against $\sqrt{\epsilon_n}$ for $E_{\rm ex} = 0$. For all $N = M$, G_f is expressed as $-\mathrm{Im}G_f(\mathrm{i}\epsilon_n) = c - b\sqrt{\epsilon_n}$ at low frequencies. Hence, $G_f(z)$ is non-analytic at $z \to +\mathrm{i}0$, and the spectrum $-\mathrm{Im}G_f(\omega + \mathrm{i}0)$ on real frequencies exhibits a cusp structure expressed by $c - b'|\omega|^{1/2}$, which has been reported for $N = M = 2$.[4,10,11] The value c at $\epsilon_n \to +0$ decreases with increasing N. From Fig. 4 and an analogy with the Friedel sum-rule in the Fermi liquid, we

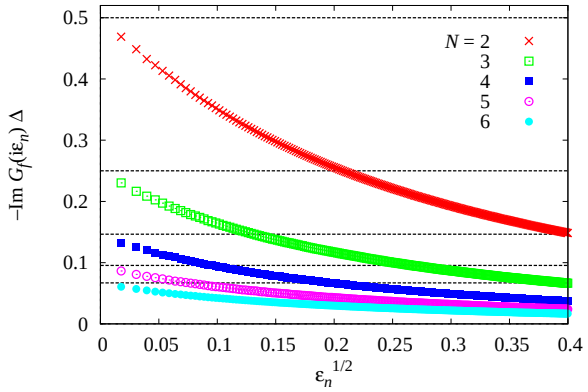

Fig. 4. (Color online) The imaginary part of the Green's function $G_f(\mathrm{i}\epsilon_n)$ for $N = M$, $NV^2 = 0.12$, $E_{\rm ex} = 0$ and $T = 0.0001$. The lines show $\sin^2(\pi/2N)$.

conjecture the following relation:

$$-\mathrm{Im}G_f(+\mathrm{i}0) = \frac{1}{\Delta}\sin^2\left(\frac{\pi}{2N}\right), \qquad (3)$$

which is indicated in Fig. 4. Eq. (3) includes the result for $N = M = 2$,[4,10,11] $1/(2\Delta)$, and reduces to the result in the non-crossing approximation,[3] $\pi^2/[(N+M)^2\Delta]$, in the limit $N = M \gg 2$. For $E_{\rm ex} = 0$, the particle-hole symmetry leads to $\mathrm{Re}G_f(\mathrm{i}\epsilon_n) = 0$, meaning that the phase shift ϕ of conduction electrons at $\omega = 0$ is fixed at $\phi = \pi/2$ irrespective of the value of $N = M$. Hence, the sine factor in eq. (3) is not connected with ϕ but is due to the imaginary part of the self-energy.

3.2 *Self-Energy*

We discuss the self-energy in the restricted Hilbert space. The self-energy $\Sigma_f(\mathrm{i}\epsilon_n)$ in the ordinary definition is given by

$$G_f(\mathrm{i}\epsilon_n) = \frac{1}{\mathrm{i}\epsilon_n - \epsilon_f - \Gamma(\mathrm{i}\epsilon_n) - \Sigma_f(\mathrm{i}\epsilon_n)}, \qquad (4)$$

where $\Gamma(\mathrm{i}\epsilon_n) = N_0^{-1}\sum_{\boldsymbol{k}} V^2/(\mathrm{i}\epsilon_n - \epsilon_{\boldsymbol{k}})$. In the restricted Hilbert space, $\Sigma_f(\mathrm{i}\epsilon_n)$ diverges according to $\Sigma_f(\mathrm{i}\epsilon_n) \sim \mathrm{i}\epsilon_n(1 - 1/a)$ at $\epsilon_n \to \infty$, since $G_f(\mathrm{i}\epsilon_n) \sim a/\mathrm{i}\epsilon_n$ with $a < 1$. Although this divergence does not produce any problem with analysis of low-energy properties, it is not convenient in practice. Thus, we define an alternative self-energy $\tilde{\Sigma}_f$ as follows:

$$G_f(\mathrm{i}\epsilon_n) = \frac{a}{\mathrm{i}\epsilon_n - \tilde{\epsilon}_f - a\Gamma(\mathrm{i}\epsilon_n) - \tilde{\Sigma}_f(\mathrm{i}\epsilon_n)}. \qquad (5)$$

$\tilde{\Sigma}_f$ is related to the ordinary self-energy Σ_f by $\tilde{\Sigma}_f = a\Sigma_f + \mathrm{i}\epsilon_n(1-a) - (\tilde{\epsilon}_f - a\epsilon_f)$, and converges in proportion to $1/\mathrm{i}\epsilon_n$ at high frequencies. By using $\tilde{\Sigma}_f$, for example, the renormalization factor z in the Fermi-liquid state is evaluated as

$$\begin{aligned} z &= [1 - \partial \mathrm{Im}\Sigma_f(\mathrm{i}\epsilon_n)/\partial\epsilon_n]^{-1}_{\epsilon_n\to+0} \\ &= a[1 - \partial \mathrm{Im}\tilde{\Sigma}_f(\mathrm{i}\epsilon_n)/\partial\epsilon_n]^{-1}_{\epsilon_n\to+0} \equiv a\tilde{z}. \end{aligned} \qquad (6)$$

$\tilde{z}$ stands for a quasi-particle weight within the restricted Hilbert space, and accordingly $\tilde{\Sigma}_f$ in eq. (5) may be a reasonable definition.

Figure 5(a) shows $-\mathrm{Im}\tilde{\Sigma}_f(\mathrm{i}\epsilon_n)$ divided by $a\Delta$ as a func-

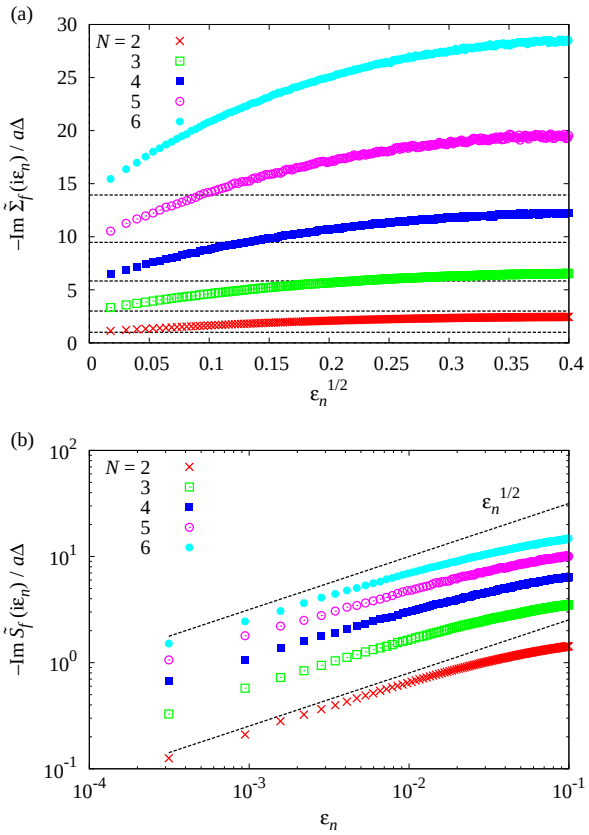

Fig. 5. (Color online) (a) The imaginary part of the self-energy $\tilde{\Sigma}_f(\mathrm{i}\epsilon_n)$ defined by eq. (5). The lines show $\cot^2(\pi/2N)$. (b) $\tilde{S}_f(\mathrm{i}\epsilon_n) = \tilde{\Sigma}_f(\mathrm{i}\epsilon_n) - \xi a\Gamma(\mathrm{i}\epsilon_n)$ on a log-log scale. The parameters are the same as in Fig. 4.

tion of $\sqrt{\epsilon_n}$. Similarly to $G_f(\mathrm{i}\epsilon_n)$, $\tilde{\Sigma}_f(\mathrm{i}\epsilon_n)$ includes a term proportional to $\sqrt{\epsilon_n}$ in the limit $\epsilon_n \to +0$, and converges to a finite value. To separate the zero-frequency value from $\tilde{\Sigma}_f$, we introduce a parameter ξ as follows:

$$\tilde{\Sigma}_f(\mathrm{i}\epsilon_n) = \xi a\Gamma(\mathrm{i}\epsilon_n) + \tilde{S}_f(\mathrm{i}\epsilon_n). \tag{7}$$

ξ is determined so that $\mathrm{Im}\tilde{S}_f(+\mathrm{i}0) = 0$. For $N = M$, noting that $\mathrm{Re}G_f(\mathrm{i}\epsilon_n) = 0$, we obtain from eq. (3)

$$\xi = \cot^2\left(\frac{\pi}{2N}\right). \tag{8}$$

In the case of $N = M = 2$, $\tilde{S}_f(\mathrm{i}\epsilon_n)$ eventually corresponds to the self-energy discussed in refs. 10 and 11. Figure 5(b) shows $\tilde{S}_f(\mathrm{i}\epsilon_n)$ on a log-log scale. We can clearly see the power-law behavior $-\mathrm{Im}\tilde{S}_f(\mathrm{i}\epsilon_n) \propto |\epsilon_n|^{1/2}$, which means $-\mathrm{Im}\tilde{S}_f(\omega + \mathrm{i}0) \propto |\omega|^{1/2}$.

3.3 Effect of Level Splitting E_{ex}: Energy Scale

So far, we have examined $E_{\mathrm{ex}} = 0$. We now discuss the effect of E_{ex}. In refs. 10 and 11, it is reported for $N = M = 2$ that $\mathrm{Im}G_f(+\mathrm{i}0)$ and $\mathrm{Im}\tilde{\Sigma}_f(+\mathrm{i}0)$ do not depend on E_{ex}. We have confirmed for $N = M \geq 2$ that eqs. (3) and (8) hold up to $E_{\mathrm{ex}} = 0.3$ within numerical accuracy. The finite value of E_{ex} causes an asymmetry of the cusp keeping the value at $\omega = 0$: $c + b|\omega|^{1/2}$ changes into $c + [b_+\theta(\omega) + b_-\theta(-\omega)]|\omega|^{1/2}$.

As E_{ex} increases, the energy scale becomes smaller. We

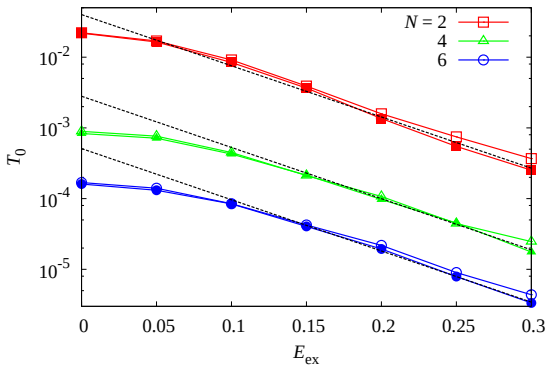

Fig. 6. (Color online) A characteristic energy scale T_0 defined in eq. (9) as a function of E_{ex}. T_0 is evaluated from $\tilde{S}_f(\mathrm{i}\epsilon_0)$ at $T = 0.0005$ (open symbols) and $T = 0.00025$ (closed symbols). The lines show $\exp[-E_{\mathrm{ex}}/NV^2\rho(0)]$.

define a characteristic energy scale T_0 in terms of $\tilde{S}_f$ by

$$-\mathrm{Im}\tilde{S}_f(\mathrm{i}\epsilon_n)/a\Delta \sim (\epsilon_n/T_0)^{1/2}, \tag{9}$$

in the limit $\epsilon_n \to 0$. Because T_0 may be defined with an arbitrary factor, we shall discuss only its exponent. In Fig. 6, we show T_0 as a function of E_{ex}. T_0 follows $T_0 \propto T_{\mathrm{K}} \propto \exp(-1/g)$ with $g = NV^2\rho(0)/E_{\mathrm{ex}}$ for $E_{\mathrm{ex}} \gtrsim 0.15$, namely $g \lesssim 0.4$. We conclude that the exponent of the energy scale of the non-Fermi liquid self-energy agrees with the Kondo temperature T_{K} in the corresponding single-channel model.

4. Summary

We have presented the impurity Green's function $G_f(\mathrm{i}\epsilon_n)$ and the self-energy $\tilde{\Sigma}_f(\mathrm{i}\epsilon_n)$ in the non-Fermi liquid state using the CT-QMC extended to the multichannel Anderson model. For $N = M$, G_f and $\tilde{\Sigma}_f$ are non-analytic at $\omega = 0$ as $|\omega|^{1/2}$. The zero-frequency spectrum $\mathrm{Im}G_f(+\mathrm{i}0)$ does not depend on the excitation energy E_{ex}, and correspondingly $\mathrm{Im}\tilde{\Sigma}_f(+\mathrm{i}0)$ has a finite value. These values depend only on N $(= M)$, and seem to be expressed as eqs. (3), (7) and (8). An analysis of general N, M is left for future work.

We acknowledge Prof. Y. Kuramoto for comments on the manuscript. This work was supported by a Grant-in-Aid for Scientific Research on Innovative Areas "Heavy Electrons" (No. 20102008) of the Ministry of Education, Culture, Sports, Science, and Technology, Japan.

1) P. Nozières and A. Blandin: J. Phys. (Paris) **41** (1980) 193.
2) D. L. Cox and A. Zawadowski: Adv. Phys. **47** (1998) 599.
3) D. L. Cox and A. E. Ruckenstein: Phys. Rev. Lett. **71** (1993) 1613.
4) A. W. W. Ludwig and I. Affleck: Phys. Rev. Lett. **67** (1991) 3160; I. Affleck and A. W. W. Ludwig: Phys. Rev. B **48** (1993) 7297.
5) A. Jerez, N. Andrei, and G. Zaránd: Phys. Rev. B **58** (1998) 3814.
6) K. Yamada: *Electron Correlation in Metals* (Cambridge University Press, Cambridge, U.K., 2004).
7) K. Yosida: *Theory of Magnetism* (Springer-Verlag, Berlin, 1996).
8) A. Schiller, F. B. Anders, and D. L. Cox: Phys. Rev. Lett. **81** (1998) 3235.
9) C. J. Bolech and N. Andrei: Phys. Rev. B **71** (2005) 205104.
10) F. B. Anders: Phys. Rev. B **71** (2005) 121101.
11) H. Johannesson, C. J. Bolech and N. Andrei: Phys. Rev. B **71** (2005) 195107.
12) J. Kroha, P. Wölfle, and T. A. Costi: Phys. Rev. Lett. **79** (1997) 261; J.

Kroha and P. Wölfle: Acta Phys. Pol. B **29** (1998) 3781.
13) A. Tsuruta, Y. Ono, T. Matsuura, and Y. Kuroda: J. Phys. Soc. Jpn. **66** (1997) 3528.
14) A.N. Rubtsov, V.V. Savkin and A.I. Lichtenstein: Phys. Rev. B **72** (2005) 035122.
15) P. Werner, A. Comanac, L.de' Medici, M. Troyer and A.J. Millis: Phys. Rev. Lett. **97** (2006) 076405; P. Werner and A.J. Millis: Phys. Rev. B **74** (2006) 155107.
16) J. Otsuki, H. Kusunose, P. Werner and Y. Kuramoto: J. Phys. Soc. Jpn. **76** (2007) 114707.